Atmospheric forcing of the oceanic semidiurnal tide

Brian K. Arbic

Program in Atmospheric and Oceanic Sciences, Princeton University, Princeton, New Jersey, USA

Received 4 October 2004; revised 28 November 2004; accepted 27 December 2004; published 29 January 2005.

[1] The principal solar semidiurnal tide (S_2) in the ocean is forced by the pressure loading of the atmospheric thermal tide as well as by the gravitational tidal potential. This paper examines the effects of adding the atmospheric S_2 forcing to a forward tide model. When the model is forced only by the gravitational potential, the S_2 relative elevation error with respect to pelagic tide gauges is anomalously poor. After atmospheric S_2 forcing is added, the relative error reduces to levels seen in other tidal constituents. In the global average, the atmospherically forced S_2 ocean tide is 14.7 percent as large as the gravitationally forced S_2 tide, and differs by about 109.4° in phase, consistent with the relative amplitudes and phases of the atmospheric and gravitational S_2 forcings. Because the S_2 air tide is periodic, the oceanic S_2 tide represents a particularly clean test of the ability of numerical models to successfully replicate the oceanic response to atmospheric pressure loading. **Citation:** Arbic, B. K. (2005), Atmospheric forcing of the oceanic semidiurnal tide, *Geophys. Res. Lett.*, *32*, L02610, doi:10.1029/2004GL021668.

1. Introduction

[2] High-frequency sea level variability is forced primarily by the gravitational tidal potential [*Munk and Cartwright*, 1966] and by atmospheric pressure loading and winds [*Ponte*, 1994]. Global observations of sea level are provided by satellite altimeters such as TOPEX/POSEIDON and JASON-1. The 10-day orbit times of these satellites lead to aliasing of high-frequency oceanic motions [*Stammer et al.*, 2000; *Tierney et al.*, 2000]. Because tides and the altimeter orbits are both periodic, tides remain periodic in the aliased altimeter record [*Parke et al.*, 1987]. Advantage is taken of this to extract tides from altimetric data. The high accuracy of open-ocean surface elevations in tide models derived from or constrained by altimetric data has been verified [*Shum et al.*, 1997] by comparison to a set of 102 pelagic tide gauges. The elevation accuracy of forward tide models, that is, hydrodynamical tide models that run unconstrained by data, is not as high as that in altimeter-constrained models. However, recently forward models have been improved with the inclusion of parameterizations of internal wave drag of topographic origin [*Jayne and St. Laurent*, 2001; *Carrère and Lyard*, 2003; *Egbert et al.*, 2004; *Arbic et al.*, 2004 (hereinafter referred to as AGHS)]. The drag schemes are motivated by inferences from both altimetric [*Egbert and Ray*, 2003] and in-situ [*Polzin et al.*, 1997] data of enhanced dissipation in regions where the seafloor is rough.

[3] Since high-frequency atmospheric fluctuations are in general not periodic, hydrodynamical models [*Fukumori et al.*, 1998; *Stammer et al.*, 2000; *Tierney et al.*, 2000; *Hirose et al.*, 2001; *Carrère and Lyard*, 2003; *Stepanov and Hughes*, 2004] must be used to remove atmospherically driven sea-level variability from altimeter data. High quality models are needed to remove both tides and atmospherically driven sea-level variability from GRACE, which measures bottom pressures from an orbit that is not periodic. The GRACE satellite mission thus provides motivation for models [*Carrère and Lyard*, 2003; *Stepanov and Hughes*, 2004] that are simultaneously forced by the atmosphere and by the gravitational tidal potential. In such models, one might also consider adding topographic drag, which *Hirose et al.* [2001] and *Carrère and Lyard* [2003] demonstrate improves the accuracy of simulated atmospherically driven sea-level variability.

[4] In the forward tide model of AGHS, driven only by the gravitational potential, the S_2 relative elevation error with respect to the pelagic tide gauges is anomalously large compared to those of other constituents. The suggestion is that physics specific to the S_2 frequency is missing from the model. The thermally forced atmospheric tides [*Lindzen*, 1990], also called "air tides", provide regular forcing of the ocean at periods of half a solar day (S_2) and of a solar day (S_1), on top of the S_2 and S_1 forcings present in the gravitational potential. The pressure loading of the atmospheric S_1 tide is the primary forcing of the small oceanic S_1 tide, which was mapped on a global scale for the first time in *Ray and Egbert* [2004]. In contrast, the oceanic S_2 tide is forced mainly by the gravitational potential and secondarily by the atmosphere. As the second largest tide in the ocean, S_2 has been mapped on a global scale in numerous altimeter-constrained models. Here we examine the effects of adding the atmospheric S_2 forcing to the AGHS tide model. We test whether such an addition improves the accuracy of the forward modeled S_2 ocean tide. We also separate the atmospherically and gravitationally forced components of S_2, and relate differences in their amplitudes and phases to differences in the respective forcings. The S_2 air tide is aliased in the atmospheric pressure products put out by analysis centers, unless special processing is introduced [*Ray and Ponte*, 2003, and references therein]. Thus, to the best of our knowledge, previous models of atmospherically driven sea-level variability do not well represent the atmospherically forced S_2 ocean tide. This tide is well represented here because we use the *Ray and Ponte* [2003] S_2 air tide map. Since the oceanic S_2 tide is periodic and well known, it presents a uniquely simple test of the ability of dynamical models to reproduce the sea level response to atmospheric pressure loading, and to simultaneously capture gravitationally and atmospherically driven sea-level variability.

2. Model, Forcings, and Diagnostics

[5] We use the one- and two-layer shallow-water models of AGHS, forced by the four largest semidiurnal (M_2, S_2,

0094-8276/05/2004GL021668$05.00

N_2, and K_2) and four largest diurnal (K_1, O_1, P_1, and Q_1) constituents, and run on a 1/2° latitude-longitude grid from 86°S to 82°N. A topographic drag scheme (*Garner* [2005] and appendix of AGHS) was tuned to minimize the misfit between modeled and altimetric surface elevations of M_2, the largest tidal constituent. Such a tuning will be optimal or nearly so for other semidiurnal tides, since the frequency dependence in the drag scheme is weak. In the current study, the forcing term in the governing momentum equation is $-g\nabla(\eta - \eta_{EQ} - \eta_{ATM} - \eta_{SAL})$, where g is gravitational acceleration, η is the model perturbation surface elevation, η_{EQ} is the gravitational tidal forcing modified to account for solid earth body tides, and η_{SAL} is the self-attraction and loading term. The new term $\eta_{ATM} = -P/\rho g$ [*Gill*, 1982], where ρ is mean seawater density and P is the annual mean atmospheric S_2 pressure map [*Ray and Ponte*, 2003], based on 13 years of operational analysis fields. *Ray and Ponte* [2003] compute an RMS discrepancy, between their map and a set of ground truth stations, of 112 microbars, much less than the 574 microbar globally averaged signal. The globally averaged signal of the *Ray and Ponte* [2003] S_2 map differs from that of the S_2 map derived from station data by *Dai and Wang* [1999] by only five percent. The argument of *Ray and Egbert* [2004], that the wind stress forcing by the S_1 atmospheric tide is negligible compared to its pressure loading, applies to S_2 as well.

[6] We will decompose periodic fields into amplitudes A and phases Φ. The S_2 component of the gravitational forcing is $\eta_{EQ-S_2} = A_{grav}(\lambda, \theta)\cos[\omega t - \Phi_{grav}(\lambda, \theta)]$, where ω is the S_2 frequency, t is time (referenced, as is the phase, to Greenwich), and λ/θ are longitude/latitude. Amplitudes A_{grav} are maximum at, and symmetric around, the equator. This is approximately true of η_{ATM} as well, with the largest values occurring in the eastern equatorial Pacific [*Ray and Ponte*, 2003, Figure 5]. Over the global ocean, the ratio of the globally averaged gravitational to atmospheric S_2 forcings is 7.09. Along lines of constant longitude, Φ_{grav} is constant. Outside of high latitudes, this is also nearly true of the atmospheric forcing [*Ray and Ponte*, 2003, Figure 5]. To estimate the difference between the phases of the two forcing fields, we computed $\int\int \sin^2[\Phi_{atm}(\lambda, \theta) - \Phi_{grav}(\lambda, \theta) - \Phi_0]\, dA$ over the global ocean, where dA is an element of area and $\Phi_{atm}(\lambda, \theta)$ is the phase of η_{ATM}, for many different values of the constant Φ_0. The integral is minimized when Φ_0 is either 110.5° or 290.5°, and we eliminate 290.5° as a possibility after inspecting scatter plots of Φ_{atm} versus Φ_{grav}.

[7] We define the model elevation discrepancy versus the pelagic tide gauges as

$$D = \sqrt{\frac{1}{N}\sum_N \left\langle (\eta - \eta_{TG})^2 \right\rangle}, \tag{1}$$

where η_{TG} is the tide gauge elevation, N is the number of tide gauge records, and brackets denote time averaging. The tide gauge signal is

$$S_{gauge} = \sqrt{\frac{1}{N}\sum_N \left\langle \eta_{TG}^2 \right\rangle}. \tag{2}$$

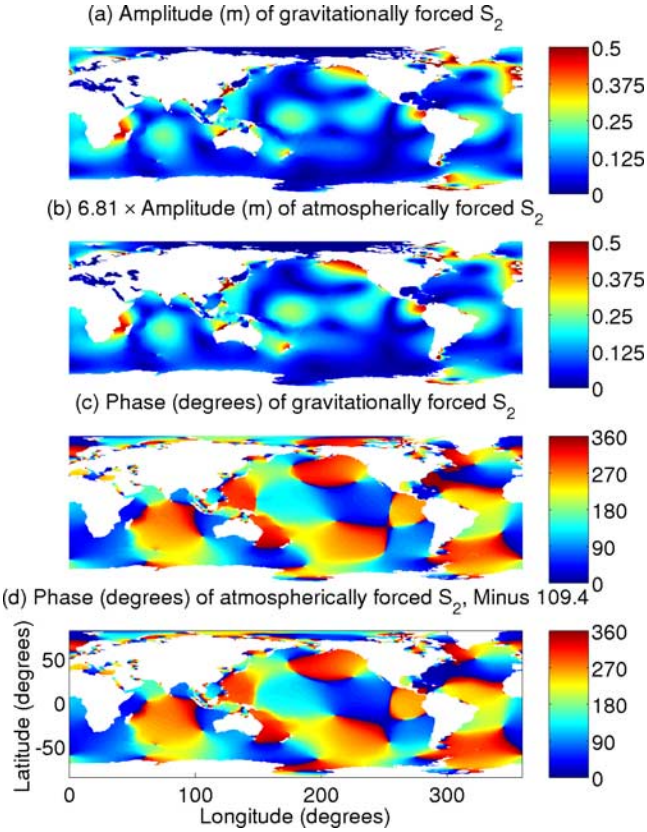

Figure 1. Amplitudes and Greenwich phases of gravitationally and atmospherically forced S_2 elevations in our one-layer forward model. We have multiplied the amplitude of the atmospherically forced component by 6.81, and subtracted 109.4° from the phase.

RSS denotes root-sum-square results computed across all constituents. The percent variance captured is $100*[1 - (D/S_{gauge})^2]$. Globally averaged signals of our modeled tides (or of altimetry-constrained models) are computed as

$$S_{arealaverage} = \sqrt{\frac{\left\langle \int\int \eta^2\, dA \right\rangle}{\int\int dA}}, \tag{3}$$

while those of the S_2 forcings are computed from (3), but with η replaced by η_{EQ-S_2} or η_{ATM} as appropriate.

3. Results and Discussion

[8] Figures 1a and 1c display the amplitude and phase maps of S_2 elevations in our one-layer model forced only by gravitational potentials. Figures 1b and 1d show the amplitude and phase of the atmospherically driven S_2 tidal elevations, taken as the difference between those in the one-layer solution forced by both η_{EQ} and η_{ATM} and those in the one-layer gravity-only solution. The globally averaged RMS signal of the atmospherically forced S_2 tide is 1.60 cm, larger than the 0.6 cm oceanic S_1 signal [*Ray and Egbert*, 2004]. The amplitude map of the atmospherically forced S_2 component has been scaled upwards by 6.81, which is the ratio of the globally averaged gravitationally forced to atmospherically forced S_2 signals. By the method previously described, the phases of the atmospherically and gravita-

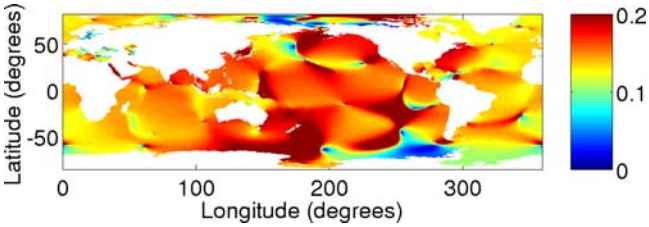

Figure 2. Ratio of amplitudes of the atmospherically to gravitationally forced S_2 ocean tide.

tionally forced S_2 tides are found to differ by 109.4°, nearly the same as the phase difference in the forcing fields. In Figure 1d we therefore subtract 109.4° from the phases of the atmospherically forced S_2 tide. The near equality of the response ratio to the forcing ratio of 7.09, and the visual similarity of the amplitude and phase maps (once adjusted appropriately), suggest that the atmospheric and gravitational S_2 forcings, which have similar spatial structures, excite the oceanic normal modes [*Platzman et al.*, 1981] in almost the same way. In contrast, *Ray and Egbert* [2004] show that the oceanic S_1 tide is markedly different from other oceanic diurnal tides (compare their Figures 4 and 6) because the very different spatial patterns of atmospheric S_1 forcing and diurnal gravitational forcing excite different normal modes.

[9] Since $\cos(\omega t) + (1/6.81)\cos(\omega t - 109.4°) = 0.96\cos(\omega t - 8.3°)$, the total S_2 tide is reduced in amplitude by a factor $R = 0.96$ and shifted in phase by $r = 8.3°$ from what it would be if forced only by the tidal gravitational potential. From an analysis of 80 tide gauges (many of which were coastal), *Cartwright and Ray* [1994] found values of $R = 0.97$ and $r = 5.9°$, but the considerable spread in values across stations covers the globally averaged values found here. The forward model also contains a wide scatter of R and r values, indicating that no simple prescription can substitute for actually including atmospheric S_2 forcing. Differences in the amplitude maps of the gravitationally and (scaled) atmospherically forced components shown in Figure 1 are visible in, for instance, the Gulf of Alaska, New Zealand, and the Weddell Sea. The nonlocality of the oceanic response (both S_2 components, for instance, are large in high latitudes, where forcings are small) makes it difficult to trace local differences in Figures 1a and 1b (or 1c and 1d) to local differences in forcing. However, rough connections can be made on basin scales. Ratios of the amplitudes of the atmospherically to gravitationally forced S_2 tide (Figure 2) are generally larger in the Pacific, where the S_2 air-tide forcing is maximum.

[10] Table 1 shows the S_2 and RSS values of pelagic tide gauge signals S_{gauge} alongside the RMS discrepancies D of

Table 1. S_2 and Root-Sum-Square (RSS) Sea-Surface Height Signals S at the Set of 102 Pelagic Tide Gauges, and Surface Height Discrepancies D of Our 1/2° Eight-Constituent One- and Two-Layer Forward Tide Simulations (Run Without S_2 Air Tide Forcing) With Respect to the Gauges[a]

Constituent	Signal S (cm)	One-Layer D (cm)	Two-Layer D (cm)
S_2	12.66	4.40 (87.9)	4.21 (88.9)
RSS	39.06	11.12 (91.9)	10.34 (93.0)

[a]Numbers in parentheses denote percentage of tide gauge sea-surface height variance captured (defined in text) in the forward simulations.

Table 2. Changes to Table 1 When the Forward Tide Simulations Include S_2 Air Tide Forcing

Constituent	Signal S (cm)	One-Layer D (cm)	Two-Layer D (cm)
S_2	12.66	3.29 (93.2)	3.10 (94.0)
RSS	39.06	10.73 (92.5)	9.94 (93.5)

our one- and two-layer forward model (forced only by gravitational potentials) with respect to the gauges. While the S_2 variance is captured at the 87.9/88.9 percent level by our one/two-layer models, the variance captured of other semi-diurnal constituents ranges from 91.4/92.2 to 92.1/93.1 percent. The S and D values in Table 1 differ by 0.04 cm from those in AGHS because here the pressure of the S_2 air tide has been removed from the bottom pressure recorder data included in the pelagic tide gauges. Table 2 shows the S_2 and RSS elevation errors in the forward models that include S_2 air-tide forcing. The S_2 percent variance captured has risen to levels seen in other semi-diurnal constituents, and the improvement in S_2 with the inclusion of air-tide forcing is much greater than the range in variance captured among the various semi-diurnal constituents. This suggests that air-tide forcing is more important than frequency sensitivities to dissipation or baroclinicity. As in the gravity-only simulations, the two layer model performs slightly better than the one-layer model when all other conditions are equal (see AGHS for more discussion.)

[11] Inclusion of the S_2 thermal tide forcing also increases the percent of the S_2 variance in the GOT99 altimetry-constrained model [*Ray*, 1999] explained by our one/two layer model, from 83.8/84.8 to 88.5/89.3 (in waters deeper than 1000 m and equatorward of 66°). The percent of S_2 variance captured with respect to GOT00, a model that estimates S_2 more reliably (R. Ray, personal communication, 2004), is slightly higher. Addition of S_2 air-tide forcing does not affect the percent of the GOT99 K_2 (mixed lunar-solar semidiurnal) variance captured in our one/two layer model (86.8/87.6). The other six constituents are captured at 91.6/92.6 percent or better. We do not understand why, even after S_2 air tide forcing is utilized, our forward modeled S_2 and K_2 remain anomalously poor with respect to GOT99. *Cartwright and Ray* [1994] and *Egbert and Ray* [2003] point out that S_2 is problematic in altimeter-constrained models, and the former points out that problems with S_2 leak into the nearby frequency K_2. The work here suggests that including the air tide forcing might improve satellite-constrained hydrodynamical tide models. However, the latter have already been validated to high accuracy against the pelagic tide gauges. We conclude by noting that K_2 also experiences an air tide forcing [*Cartwright and Tayler*, 1971]. However, to our knowledge, maps of the K_2 air tide are not readily available. We estimate that K_2 air tide forcing would change the oceanic K_2 tide by about 4.7 percent, a substantially smaller correction than for S_2.

[12] **Acknowledgments.** Rui Ponte, Gary Egbert, and Steve Jayne are thanked for pointing out the anomalous nature of the S_2 ocean tide. Laurie Padman is thanked for suggesting in his review of AGHS that the forward tide model be measured against tide gauges as well as against altimetry. Doug Luther, Gabriel Lau, Arlene Fiore, Steve Jayne, and an anonymous reviewer are thanked for helpful comments on the manuscript. DL pointed out the existence of K_2 air tide forcing. Richard Ray is especially thanked, for several illuminating discussions, for providing his maps of the S_2 air tide, and for useful comments on the manuscript. Jeff Forbes, Maura Hagan,

Larry Horowitz, Steve Garner, Baylor Fox-Kemper, Anand Gnanadesikan, Pablo Zurita, Olivier Pauluis, Bob Hallberg, Andrew Wittenberg, and Aiguo Dai are also thanked for helpful discussions. Support from National Science Foundation Grant OCE-0327189 is gratefully acknowledged. Computations were done on the supercomputer at the Geophysical Fluid Dynamics Laboratory (GFDL) of the National Oceanic and Atmospheric Administration (NOAA).

References

Arbic, B. K., S. T. Garner, R. W. Hallberg, and H. L. Simmons (2004), The accuracy of surface elevations in forward global barotropic and baroclinic tide models, *Deep Sea Res., Part II*, *51*, 3069–3101.

Carrère, L., and F. Lyard (2003), Modeling the barotropic response of the global ocean to atmospheric wind and pressure forcing: Comparisons with observations, *Geophys. Res. Lett.*, *30*(6), 1275, doi:10.1029/2002GL016473.

Cartwright, D. E., and R. D. Ray (1994), On the radiational anomaly in the global ocean tide with reference to satellite altimetry, *Oceanol. Acta*, *17*, 453–459.

Cartwright, D. E., and R. J. Tayler (1971), New computations of the tide-generating potential, *Geophys. J. R. Astron. Soc.*, *23*, 45–74.

Dai, A., and J. Wang (1999), Diurnal and semidiurnal tides in global surface pressure fields, *J. Atmos. Sci.*, *56*, 3874–3891.

Egbert, G. D., and R. D. Ray (2003), Semi-diurnal and diurnal tidal dissipation from TOPEX/POSEIDON altimetry, *Geophys. Res. Lett.*, *30*(17), 1907, doi:10.1029/2003GL017676.

Egbert, G. D., R. D. Ray, and B. G. Bills (2004), Numerical modeling of the global semidiurnal tide in the present day and in the Last Glacial Maximum, *J. Geophys. Res.*, *109*, C03003, doi:10.1029/2003JC001973.

Fukumori, I., R. Raghunath, and L.-L. Fu (1998), Nature of global large-scale sea level variability in relation to atmospheric forcing: A model study, *J. Geophys. Res.*, *103*, 5493–5512.

Garner, S. T. (2005), A topographic drag closure built on an analytical base flux, *J. Atmos. Sci.*, in press.

Gill, A. E. (1982), *Atmosphere-Ocean Dynamics*, 662 pp., Elsevier, New York.

Hirose, N., I. Fukumori, V. Zlotnicki, and R. M. Ponte (2001), Modeling the high-frequency barotropic response of the ocean to atmospheric disturbances: Sensitivity to forcing, topography, and friction, *J. Geophys. Res.*, *106*, 30,987–30,995.

Jayne, S. R., and L. C. St. Laurent (2001), Parameterizing tidal dissipation over rough topography, *Geophys. Res. Lett.*, *28*, 811–814.

Lindzen, R. S. (1990), *Dynamics in Atmospheric Physics*, 310 pp., Cambridge Univ. Press, New York.

Munk, W. H., and D. E. Cartwright (1966), Tidal spectroscopy and prediction, *Philos. Trans. R. Soc. London, Ser. A*, *259*, 533–581.

Parke, M. E., R. H. Stewart, D. L. Farless, and D. E. Cartwright (1987), On the choice of orbits for an altimetric satellite to study ocean circulation and tides, *J. Geophys. Res.*, *92*, 11,693–11,707.

Platzman, G. W., G. A. Curtis, K. S. Hansen, and R. D. Slater (1981), Normal modes of the world ocean. Part II: Description of modes in the period range 8 to 80 hours, *J. Phys. Oceanogr.*, *11*, 579–603.

Polzin, K. L., J. M. Toole, J. R. Ledwell, and R. W. Schmitt (1997), Spatial variability of turbulent mixing in the abyssal ocean, *Science*, *276*, 93–96.

Ponte, R. M. (1994), Understanding the relation between wind- and pressure-driven sea level variability, *J. Geophys. Res.*, *99*, 8033–8039.

Ray, R. D. (1999), A global ocean tide model from TOPEX/POSEIDON altimetry: GOT99.2, *Tech. Memo. NASA/TM-1999-209478*, 58 pp., NASA, Washington, D. C.

Ray, R. D., and G. D. Egbert (2004), The global S_1 tide, *J. Phys. Oceanogr.*, *34*, 1922–1935.

Ray, R. D., and R. M. Ponte (2003), Barometric tides from ECMWF operational analyses, *Ann. Geophys.*, *21*, 1897–1910.

Shum, C. K., et al. (1997), Accuracy assessment of recent ocean tide models, *J. Geophys. Res.*, *102*, 25,173–25,194.

Stammer, D., C. Wunsch, and R. M. Ponte (2000), De-aliasing of global high-frequency barotropic motions in altimeter observations, *Geophys. Res. Lett.*, *27*, 1175–1178.

Stepanov, V. N., and C. W. Hughes (2004), Parameterization of ocean self-attraction and loading in numerical models of the ocean circulation, *J. Geophys. Res.*, *109*, C03037, doi:10.1029/2003JC002034.

Tierney, C., J. Wahr, F. Bryan, and V. Zlotnicki (2000), Short-period oceanic circulation: Implications for satellite altimetry, *Geophys. Res. Lett.*, *27*, 1255–1258.

B. K. Arbic, Program in Atmospheric and Oceanic Sciences, Princeton University, P.O. Box CN710, Sayre Hall, Princeton, NJ 08544-0710, USA. (arbic@splash.princeton.edu)